Sodium Ion Diffusion and Voltage Trends in Phosphates Na$_4$M$_3$(PO$_4$)$_2$P$_2$O$_7$ (M = Fe, Mn, Co, Ni) for Possible High-Rate Cathodes

Stephen M. Wood,[†] Chris Eames,[†] Emma Kendrick,[‡,§] and M. Saiful Islam*,[†]

[†]Department of Chemistry, University of Bath, Claverton Down, Bath BA2 7AY, United Kingdom
[‡]SHARP Laboratories of Europe Limited, Oxford OX4 4GB, United Kingdom
[§]School of Chemistry, University of Birmingham, Edgbaston, Birmingham B15 2TT, United Kingdom

Ⓢ Supporting Information

ABSTRACT: Polyanionic phosphates have the potential to act as low-cost cathodes and stable framework materials for Na ion batteries. The mixed phosphates Na$_4$M$_3$(PO$_4$)$_2$P$_2$O$_7$ (M = Fe, Mn, Co, Ni) are a fascinating new class of materials recently reported to be attractive Na ion cathodes which display low-volume changes upon cycling, indicative of long-lifetime operation. Key issues surrounding intrinsic defects, Na ion migration mechanisms, and voltage trends have been investigated through a combination of atomistic energy minimization, molecular dynamics (MD), and density functional theory simulations. For all compositions, the most energetically favorable defect is calculated to be the Na/M antisite pair. MD simulations suggest Na$^+$ diffusion extends across a 3D network of migration pathways with an activation barrier of 0.20−0.24 eV, and diffusion coefficients (D_{Na}) of 10^{-10}−10^{-11} cm^2 s^{-1} at 325 K, suggesting good rate capability. The voltage trends indicate that doping the Fe-based cathode with Ni can significantly increase the voltage, and hence the energy density.
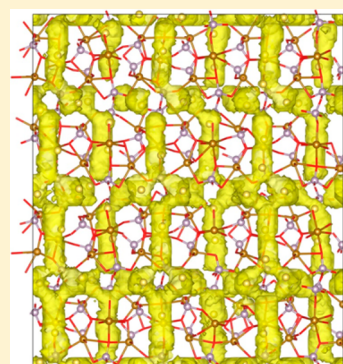
1. INTRODUCTION

Rechargeable lithium batteries have come to dominate portable energy storage over the past two decades, primarily due to their light weight and high energy density.[1,2] However, there are concerns over the abundance and cost of lithium, and the safety of Li ion batteries. Na ion batteries have been touted as alternatives to Li ion batteries because of a higher natural abundance, and lower cost of sodium, as well as its intercalation chemistry being similar to that of lithium.[3−8] Hence, there is renewed interest in electrode materials that can easily intercalate and transport Na ions at suitable potentials.

Electrode selection is critical in the development of Na ion batteries, and cathode materials research has followed strategies similar to that of Li ion battery systems. Various layered oxide compounds have attracted attention, including Na$_{0.44}$MnO$_2$,[9,10] Na$_x$CoO$_2$,[11] Na$_x$[Fe$_{0.5}$Mn$_{0.5}$]O$_2$,[12] and Na$_{0.85}$Li$_{0.17}$Ni$_{0.21}$-Mn$_{0.64}$O$_2$.[13] These materials have an advantage over their lithium analogues as the larger ionic radius of the Na$^+$ ion inhibits transformations to spinel polymorphs upon cycling, which leads to improved stability. However, a rich variety of intermediate phases leads to an intricate set of phase transitions upon cycling, adding to the complexity of ion migration upon charge/discharge.[14,15]

Polyanionic cathodes have also garnered notable recent interest. These materials typically demonstrate better capacity retention and cycle stability than layered oxides, due to their robust and stable frameworks with tightly bound polyanions. In addition, the voltage response upon cycling is generally simpler

than that of layered oxides, as two-phase behavior, with a well-defined phase boundary, is usually favored.[16] Polyanionic materials of interest include Na superionic conductor (NASICON)-type compounds (such as Na$_3$V$_2$(PO$_4$)$_3$),[17] NaVPO$_4$F,[18] NaFePO$_4$,[19−21] and Na$_2$FePO$_4$F.[16,22−24]

More recently, mixed phosphates of the general formula Na$_4$M$_3$(PO$_4$)$_2$P$_2$O$_7$ (where M is a transition metal) have been considered as potential cathodes. The Co system Na$_4$Co$_3$-(PO$_4$)$_2$P$_2$O$_7$ has been synthesized through a sol−gel process by Nose et al.[25] and was shown to reversibly intercalate Na ions at high voltage (∼4.7 V), with a capacity of ca. 99 mA h g^{-1} at a 0.2C rate. Furthermore, the material demonstrated excellent rate performance, retaining an 89 mA h g^{-1} capacity at a 5C rate.[25] The Na$_4$Fe$_3$(PO$_4$)$_2$P$_2$O$_7$ material has been studied by Kang et al.[26,27] using combined experimental and density functional theory (DFT) techniques. A theoretical capacity of 129 mA h g^{-1} delivered at approximately 3.2 V vs Na/Na$^+$ is competitive with those of other Na ion cathodes.[8]

It has been shown that Na$_4$Fe$_3$(PO$_4$)$_2$P$_2$O$_7$ does not undergo a phase change upon Na ion extraction, with a small volume change of just 4% upon cycling. This value compares favorably with those of other Na ion battery materials, such as NaFePO$_4$ and NaFeSO$_4$F, which exhibit a volume change of 15% and 14.5%, respectively, upon cycling.[16,28] The low volume change

in $Na_4Fe_3(PO_4)_2P_2O_7$ is important for good long-term cycle life.[26,27]

Our focus here is in probing the defect, diffusion, and voltage trends of the $Na_4M_3(PO_4)_2P_2O_7$ (M = Fe, Mn, Co, Ni) class of materials. In this study, we have applied a combination of atomistic energy minimization and molecular dynamics methods to examine the processes governing the defect chemistry and ion migration. In addition, we have employed DFT methods to study the trends in cell voltage across a variety of transition-metal configurations.

2. METHODS

Atomistic modeling techniques have been widely used in the study of defect and transport properties of solids. These have been detailed elsewhere,[8,29−31] and as such only a brief outline will be given here.

Interatomic interactions were represented by a long-range electrostatic term plus a function representing the short-range repulsive and van der Waals interactions. Since charged defects will polarize other ions in the lattice, it is important to incorporate electronic polarization into the potential model, and this was achieved through inclusion of the shell model.[29,30] A crucial feature of defect simulations is the treatment of lattice relaxation about the charged defect or migrating Na^+ ion. The Mott−Littleton approach was used, whereby the crystal lattice is partitioned into two regions, implemented through the GULP code.[30] This approach has previously been used effectively to explore a number of battery materials.[16,32−36]

Molecular dynamics (MD) simulations were performed with DL_POLY (version 4)[37] using a fitted version of the partial-charge potential model of Pedone et al.,[38] which has been explicitly developed to allow rapid simulation of finite temperature properties in complex oxides. An overview of the potentials and structural reproduction from this model is given in Tables S1 and S2 (Supporting Information). A supercell consisting of 10 × 4 × 6 unit cells (~25000 ions) was used, with 5% of Na ions removed randomly. The systems were pre-equilibrated for at least 750 ps (with a time step of 1.5 fs) before the main simulation runs of 750 ps were performed. An NPT ensemble, with a Berendson thermostat, was used throughout to allow for thermal expansion. Sodium ion diffusion coefficients were calculated from the mean square displacements. Such MD techniques have previously been applied to many lithium battery and solid oxide fuel cell ion conductors.[39−43]
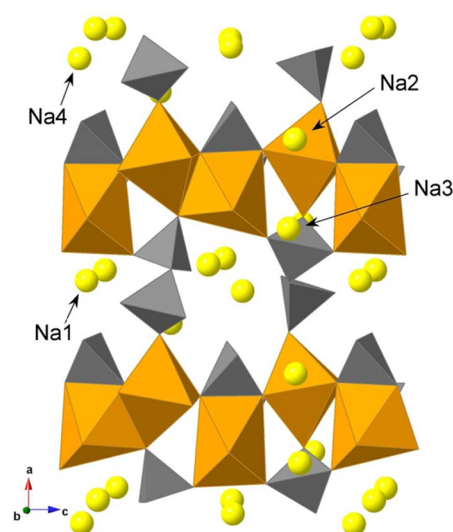
Figure 1. Experimental structure of $Na_4Fe_3(PO_4)_2P_2O_7$ as a representative system for all materials studied. FeO_6 units are brown, PO_4 and P_2O_7 units are gray, and Na^+ ions are yellow.

DFT calculations were performed using a plane wave basis set implemented in the VASP code.[44] A cutoff energy of 800 eV and a k-point grid of 1 × 2 × 2 were needed to adequately converge the forces and energies. PAW potentials[45,46] and spin-polarized generalized gradient approximation (GGA) with the PBESol functional[47] were used. DFT+U methodology was used to account for the metal d-orbitals with an effective Hubbard $U_{eff} = U − J = 4.3, 3.9,$ and 6.0 eV ($J = 1.0$ eV) for Fe, Mn, and Ni, respectively. These values are consistent with those previously derived for cathode materials.[48] See the Supporting Information (Table S3) for a tabulated list of published U values from battery cathode studies. In addition, van der Waals interactions were considered as these have been shown to influence cell voltage in some polyanionic systems.[49] However, for these materials, they were found to have a negligible effect on calculated voltages, probably due to the paucity of unscreened dispersion interactions.

Previous DFT studies on a range of oxide electrode materials[50,51] have shown such methods to be well suited to simulating precise trends in cell voltages. For all materials the Na^+/Na cell voltages for the M^{2+}/M^{3+} redox couples were calculated from

$$V = \frac{\varepsilon\{Na_4M_3(PO_4)_2P_2O_7\} - \varepsilon\{Na_xM_3(PO_4)_2P_2O_7\} - (4 - x)\mu\{Na\}}{4 - x}$$

(1)

where $\varepsilon\{Y\}$ is the total energy of composition Y and x is the number of sodium atoms remaining per formula unit, which was taken as $x = 1$ to produce the end member $NaM_3(PO_4)_2$-P_2O_7. The chemical potential of sodium, $\mu\{Na\}$, was calculated using metallic sodium, which is standard practice for cell voltage calculations.

3. RESULTS AND DISCUSSION

3.1. Structures and Intrinsic Defects. The starting point for our simulations is the reproduction of the observed crystal structures. The structures of $Na_4M_3(PO_4)_2P_2O_7$ (where M = Fe, Co, Mn, Ni) all adopt a similar crystal structure with a $Pna2_1$ space group.[25,26,52] The $Na_4Fe_3(PO_4)_2P_2O_7$ structure is

shown in Figure 1. The transition metals reside in octahedral sites which are joined by phosphate $(PO_4)^{3−}$ groups to form layers in the bc plane. These layers are bridged parallel to the a axis by pyrophosphate, $(P_2O_7)^{4−}$, groups, forming a 3D framework. The Na^+ ions are found in four nonequivalent sites with Na1 and Na4 residing in two channels in the phosphate framework parallel to the b axis. The interatomic potentials for all four systems $Na_4M_3(PO_4)_2P_2O_7$ (where M = Fe, Mn, Ni, Co) were derived simultaneously, which is not trivial for such complex structures. A comparison between the calculated structures based on these effective potentials (Table S4, Supporting Information) and experimental data is given in Table 1.

Table 1. Deviation (Δ) between Calculated and Experimental Structures[26,52] of $Na_4M_3(PO_4)_2P_2O_7$ (M = Fe, Mn, Ni, and Co)

unit cell param	Fe	Mn	Ni	Co
a/Å	0.16	0.31	0.06	0.01
b/ Å	−0.01	−0.06	−0.02	0.03
c/ Å	0.10	−0.09	0.09	0.11
α/deg	0.00	0.00	0.00	0.00
β/deg	0.61	0.00	0.00	0.00
γ/deg	0.00	0.00	0.00	0.00
bond lengths				
M−O/ Å	0.127	0.077	0.062	0.050
P−O/ Å	0.116	0.102	0.100	0.092
Na−O/ Å	0.190	0.079	0.057	0.061

The calculated unit cell parameters differ from experiment by at most 1.74%, and in most cases the deviations are substantially less. The mean deviations in bond lengths are 0.071, 0.103, and 0.097 Å for the M−O, P−O, and Na−O bonds, respectively. The shorter average Na−O bond length (2.38 Å compared to 2.48 Å) found in the Fe material from experiment makes reproduction of the series of complex structures challenging when using the same Na−O and P−O potentials. Nevertheless, the accurate reproduction of all structures, including the iron analogue, with the same interatomic potentials gives us confidence that the model can be used reliably in subsequent defect and migration simulations to explore trends in properties.

To investigate the intrinsic defect chemistry, a series of isolated point defect energies (vacancy, interstitial, and impurity) were calculated for all four transition metals in $Na_4M_3(PO_4)_2P_2O_7$ (M = Fe, Mn, Ni, and Co). Combining the energies of these point defects, energies of formation for Frenkel- and Schottky-type disorder can be derived. The corresponding equations in Kroger−Vink notation are given in the Supporting Information. We also examined Na/M "antisite" pair defects involving the exchange of positions of a pair of Na^+ (radius 1.02 Å)[50] and M^{2+} (radius 0.61 Å (Fe), 0.83 Å (Mn), 0.65 Å (Co), and 0.69 Å (Ni))[53] ions. This type of defect is worth considering as it has been observed in other polyanionic battery systems, such as $NaFePO_4$ and Li_2MnSiO_4.[16,54] It has also been predicted to have a significant impact on the electrochemical performance of some materials. The defect formation results are presented in Table 2, from which three main points emerge.

First, the high energies associated with M Frenkel, O Frenkel, P Frenkel, and Schottky defects (for all transition metals) suggest that such intrinsic defects are unfavorable. Hence, such defects are unlikely to exist in significant concentrations in the undoped materials.

Table 2. Calculated Intrinsic Defect Energies (eV) for $Na_4M_3(PO_4)_2P_2O_7$ (M = Fe, Mn, Ni, and Co)

defect type	Fe	Mn	Ni	Co
Na Frenkel	1.85	1.97	2.29	1.86
O Frenkel	5.26	5.35	5.90	7.59
P Frenkel	24.11	24.26	24.35	25.43
M Frenkel	5.14	4.80	6.27	6.36
Schottky	102.55	106.54	117.80	111.02
Na/M antisite	1.19	1.37	1.72	1.44

Second, the most favorable type of intrinsic defect is predicted to be the Na/M antisite pair for all materials, as has been found in previous studies of $NaFePO_4$ and $Na_2FeP_2O_7$.[16,36] Furthermore, from the energetics, the concentration of antisite defects would be expected to be greatest in $Na_4Fe_3(PO_4)_2P_2O_7$ and least in $Na_4Ni_3(PO_4)_2P_2O_7$. This may have an impact on electrochemical performance as antisite defects have the potential to "block" sodium ion migration especially in 1D Na^+ conductors.

Third, Na Frenkel defects also have a relatively low energy, suggesting a minor intrinsic population of Na interstitials and vacancies. As with the antisite defects, the Fe-based material is predicted to have the highest defect concentration, while the Ni-based material should display the lowest defect population.

3.2. Na Ion Diffusion. Sodium diffusion properties are of vital interest when examining the electrode kinetics. Our MD simulations focused on the Fe- and Mn-based materials, as these two are of greatest practical interest because of their high natural abundance. Simulations over significant time scales and various operating temperatures have been conducted for the compositions $Na_{3.8}M_3(PO_4)_2P_2O_7$ for M = Fe and Mn.

Initially, the mean square displacement (MSD), $\langle [r(t)]^2 \rangle$, of sodium ions was resolved, and then used to derive Na ion diffusion coefficients (D_{Na}) from the relation

$$D = \frac{1}{6} \frac{d\langle [r(t)]^2 \rangle}{dt} \tag{2}$$

yielding D_{Na} values of 6.1×10^{-11} and 3.1×10^{-10} cm^2 s^{-1} at 325 K for the Fe and Mn materials, respectively. Although no experimentally measured diffusion data are available for direct comparison, these values compare well to those of other Na ion cathodes; these include layered oxides Na_xMnO_2 (10^{-11} cm^{-2} s^{-1})[55] and polyanionic materials such as $Na_3V_2(PO_4)_2F$ (10^{-10} cm^2 s^{-1}).[56] See Table S5 in the Supporting Information for a selection of Na diffusion coefficients from the published literature.

Our diffusion data can also be used to estimate activation barriers (E_a) of Na ion migration from an Arrhenius plot (ln D vs $1/T$), shown in Figure 2. A diffusion barrier of 0.2−0.24 eV is predicted for the two materials, indicative of fast Na ion
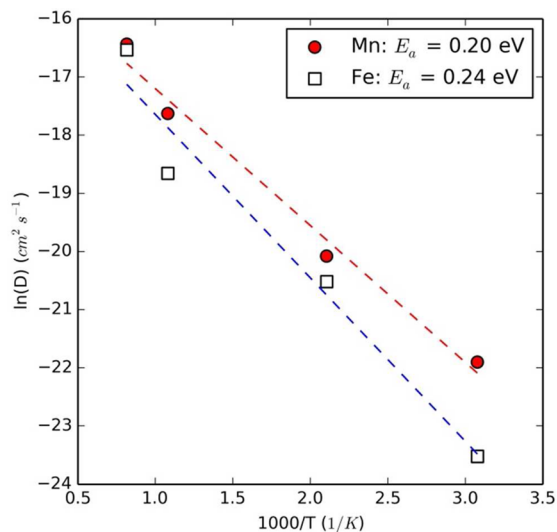
Figure 2. Arrhenius plot of Na ion diffusion coefficients in $Na_{3.8}Fe_3(PO_4)_2P_2O_7$ and $Na_{3.8}Mn_3(PO_4)_2P_2O_7$.

mobility and high rate performance in the polyanion framework. Comparable activation barriers between Li and Na ion cathodes have been found in various materials,[16,27,36,57] despite the larger ionic radius of the Na^+ ion (1.02 Å) compared to the Li^+ ion (0.76 Å).[53] This is typically rationalized by the tendency of sodium to be less polarizing than lithium and to form longer Na−O bonds, providing a more open framework structure. Previous DFT analysis[27] of the Fe material found a higher activation barrier (∼0.5 eV), although this was determined from nudged elastic band (NEB) calculations for a single migrating Na ion.

A useful means of visualizing diffusion trajectories is plotting accumulated Na ion densities, which indicates the lattice sites most frequently traversed over the course of the simulation run. These plots are shown in Figure 3 for the Fe system; we note
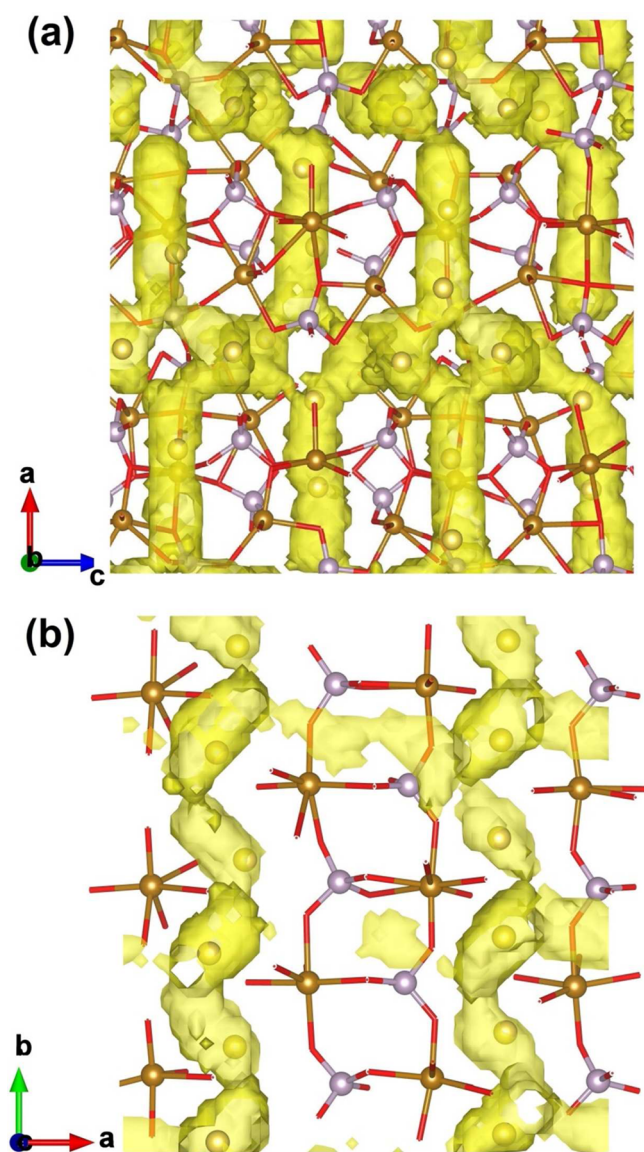
Figure 3. Na ion density plots for $Na_{3.8}Fe_3(PO_4)_2P_2O_7$ overlaid on initial lattice sites. Key: Na, yellow; Fe, brown; P, gray; O, red; yellow details Na ion migration pathways. (a) 3D network view down the b axis revealing linear regions (involving Na2 and Na3 sites) and (b) magnified view showing the curved paths along the b axis channels (involving Na1 and Na4 sites).

that the same behavior is found for the Mn-based material. The broad distribution and significant overlap of Na ion densities demonstrate the highly mobile nature of Na ions in this material involving all Na sites. This diffusion extends over a 3D network throughout the material, in which b axis channels (containing sites Na1 and Na4) are connected by intralayer migration through Na2 and Na3 sites. Within this context, the low antisite defect energy is likely to have less of an impact than would be expected in the case of 1D diffusion where it would block the 1D channel. The 3D network and low activation barriers, as well as the low volume change upon cycling, are promising features for good rate capability of these cathodes.

Closer analysis indicates that the topology of the migration paths varies throughout the diffusion network. The pathways involving only Na2 and Na3 are essentially linear; i.e., they span the shortest path trajectory, as can be seen in Figure 3a. Conversely, for diffusion involving Na1−Na1 and Na4−Na4 paths down the b axis channels, a curved trajectory is found, which provides the lowest energy pathways, as shown in Figure 3b. Such curved trajectories have also been observed in other polyanion materials, such as $NaFePO_4$.[16] The trajectories for Na ion diffusion are largely consistent with previous DFT analysis of the Fe material.[27]

3.3. Voltage Trends. Tailoring the cell voltage is key to achieving optimal battery performance and maximizing energy density. DFT calculations were thus used to explore transition-metal doping of the $Na_4Fe_3(PO_4)_2P_2O_7$ material and its influence on the cell voltage. To calculate the cell voltage, the relevant sodium ions are removed from the structure, which is subsequently energy minimized to determine the most stable structure. Numerous vacancy configurations were tested on the basis of the results of both screening using potential-based simulations and previous DFT studies.[26] The voltage was extracted from the lowest energy configurations using eq 1.

As with potential-based calculations, the $Na_4M_3(PO_4)_2P_2O_7$ (M = Fe, Ni, Mn) experimental structures have been reproduced by DFT to a high degree of accuracy (Table S6, Supporting Information). Furthermore, the cell voltage for $Na_4Fe_3(PO_4)_2P_2O_7$ is calculated to be 3.0 eV vs Na/Na^+, in good agreement with the experimental value of 3.2 V vs Na/Na^+.[27] The voltage, and energy density, of $Na_4Fe_3(PO_4)_2P_2O_7$ would generally be considered too low for optimal battery performance. Therefore, to raise the calculated voltage, doping with Mn and Ni has been explored, as both cations typically display higher voltages than Fe-containing materials.

The trend in voltage across transition-metal compositions is detailed in Figure 4 as a function of the Fe content. The transition-metal end members ($Na_4Fe_3(PO_4)_2P_2O_7$, $Na_4Mn_3(PO_4)_2P_2O_7$, and $Na_4Ni_3(PO_4)_2P_2O_7$) follow the series Fe (3.0 V) < Mn (3.5 V) < Ni (4.9 V); other battery material series such as $LiMPO_4$,[58,59] $Li_2MP_2O_7$,[60] and Na_2MPO_4F[61] are known experimentally to follow a similar pattern. In addition, the voltage of the Ni end member (4.9 eV) is outside the stability window of standard electrolytes. While the voltage of the Mn material is more attractive, Mn-based phosphates often experience problems with redox cycling typically on account of Jahn−Teller effects.

Compositions $Na_4Fe_{3−x}Mn_x(PO_4)_2P_2O_7$ (for x = 1, 2) are calculated to have a voltage of 3.2 V, suggesting Mn doping provides a relatively minor increase in cell voltage and energy density. Conversely, Ni doping is predicted to deliver a significant increase in cell voltage, providing a high degree of voltage control by varying the doping concentration.
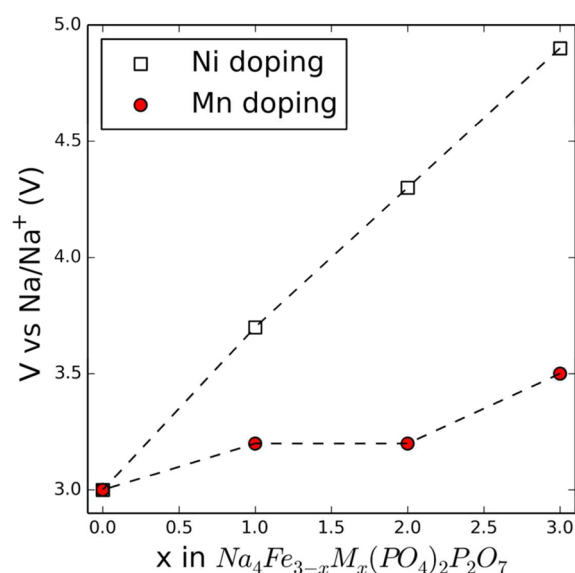
Figure 4. Trends in cell voltage (vs Na/Na$^+$) as a function of increasing Mn and Ni concentrations on the Fe site in Na$_4$Fe$_3$(PO$_4$)$_2$P$_2$O$_7$.

Furthermore, the composition Na$_4$Fe$_2$Ni(PO$_4$)$_2$P$_2$O$_7$ is predicted to have a cell voltage of 3.7 V, close to the upper limit on voltage set by typical electrolyte stability windows. Therefore, we predict that doping Na$_4$Fe$_3$(PO$_4$)$_2$P$_2$O$_7$ with a relatively modest level of Ni would lead to a ∼25% enhancement in voltage; this is a significant increase to a viable voltage in terms of energy density and electrolyte stability.

4. CONCLUSIONS

A combination of atomistic energy minimization, MD, and DFT simulation techniques has been used to provide insights into the defect chemistry, Na ion diffusion, and voltage trends in the Na ion battery materials Na$_4$M$_3$(PO$_4$)$_2$P$_2$O$_7$ (M = Fe, Mn, Ni, Co).

First, our atomistic potential model provides an accurate reproduction of the complex structures for all four compositions. In all materials the most favorable intrinsic defect is found to be the Na/M antisite pair.

Large-scale MD simulations allowed us to explore Na ion diffusion kinetics and transport mechanisms. Na$^+$ diffusion coefficients (D_{Na}) are on the order of 10^{-10}–10^{-11} cm^2 s^{-1} at 325 K, and activation barriers are found to be 0.20–0.24 eV in the Fe- and Mn-based materials. These values compare favorably to those of successful Li ion cathodes, indicating rapid Na ion transport, which, coupled with the small volume change observed on cycling, suggests high rate capability and good cycle life. In addition, the MD trajectories suggest a 3D network of migration pathways, with all sodium ions diffusing. Closer analysis indicates that all pathways involving Na2 and Na3 sites are essentially linear, while for diffusion down the b axis channels (Na1 and Na4 sites) curved trajectories are found.

Finally, DFT methods have been used to explore voltage trends. The experimental voltage of Na$_4$Fe$_3$(PO$_4$)$_2$P$_2$O$_7$ is reproduced, and higher cell voltages for Na$_4$Mn$_3$(PO$_4$)$_2$P$_2$O$_7$ and Na$_4$Ni$_3$(PO$_4$)$_2$P$_2$O$_7$ are predicted. Moreover, we demonstrated that doping Na$_4$Fe$_3$(PO$_4$)$_2$P$_2$O$_7$ with Ni can lead to a significant increase in voltage.

These results will assist in developing strategies for optimizing these novel phosphates as possible high-rate Na

ion cathodes, especially for the cost-sensitive stationary storage sector.

■ ASSOCIATED CONTENT

ⓢ Supporting Information

Potential parameters employed in simulations and deviation between calculated and experimental structures from all simulation techniques, tabulated U_{eff} values from computational studies of Li ion and Na ion battery materials, tabulated Na$^+$ diffusion coefficients from studies of Na ion battery materials, and thermodynamic stability data and calculated density of states from DFT simulations. The Supporting Information is available free of charge on the ACS Publications website at DOI: 10.1021/acs.jpcc.5b04648.

■ AUTHOR INFORMATION

Corresponding Author
*E-mail: M.S.Islam@bath.ac.uk.

Notes
The authors declare no competing financial interest.

■ ACKNOWLEDGMENTS

■ REFERENCES

(1) Tarascon, J. M.; Armand, M. Issues and Challenges Facing Rechargeable Lithium Batteries. *Nature* **2001**, *414*, 359−367.

(2) Bruce, P. G.; Scrosati, B.; Tarascon, J. M. Nanomaterials for Rechargeable Lithium Batteries. *Angew. Chem., Int. Ed.* **2008**, *47*, 2930−2946.

(3) Kim, S. W.; Seo, D. H.; Ma, X. H.; Ceder, G.; Kang, K. Electrode Materials for Rechargeable Sodium-Ion Batteries: Potential Alternatives to Current Lithium-Ion Batteries. *Adv. Energy Mater.* **2012**, *2*, 710−721.

(4) Ellis, B. L.; Nazar, L. F. Sodium and Sodium-Ion Energy Storage Batteries. *Curr. Opin. Solid State Mater. Sci.* **2012**, *16*, 168−177.

(5) Yamada, A. Iron Based Materials Strategies. *MRS Bull.* **2014**, *39*, 423−428.

(6) Yabuuchi, N.; Kubota, K.; Dahbi, M.; Komoba, S. Research Development on Sodium-Ion Batteries. *Chem. Rev.* **2014**, *114*, 11636−11682.

(7) Palomeres, V.; Casas-Cabanas, M.; Castillo-Martinez, E.; Han, M. H.; Rojo, T. Update on Na-Based Battery Materials. A Growing Research Path. *Energy Environ. Sci.* **2013**, *6*, 2312−2337.

(8) Islam, M. S.; Fisher, C. A. J. Lithium and Sodium Battery Cathode Materials: Computational Insights into Voltage, Diffusion and Nanostructural Properties. *Chem. Soc. Rev.* **2014**, *43*, 185−204.

(9) Doeff, M. M.; Peng, M. Y.; Ma, Y. P.; Dejonghe, L. C. Orthombric Na$_x$MnO$_2$ as a Cathode Material for Secondary Sodium and Lithium Polymer Batteries. *J. Electrochem. Soc.* **1994**, *141*, L145−L147.

(10) Kim, D. J.; Ponraj, R.; Kannan, A. G.; Lee, H. W.; Fathi, R.; Ruffo, R.; Mari, C. M.; Kim, D. K. Diffusion Behaviour of Sodium Ions in Na$_{0.44}$MnO$_2$ in Aqueous and Non-Aqueous Electrolytes. *J. Power Sources* **2013**, *244*, 758−763.

(11) Braconnier, J. J.; Delmas, C.; Fouassier, C.; Hagenmuller, P. Comportment Electrochimique des Phases Na$_x$CoO$_2$. *Mater. Res. Bull.* **1980**, *15*, 1797−1804.

(12) Yabuuchi, N.; Kajiyama, M.; Iwatate, J.; Nishiwaka, H.; Hitomi, S.; Okuyama, R.; Usui, R.; Yamada, Y.; Komaba, S. P2-Type $Na_x[Fe_{1/2}Mn_{1/2}]O_2$ Made from Earth-Abundant Elements for Rechargeable Na Batteries. *Nat. Mater.* **2012**, *11*, 512−517.

(13) Kim, D.; Kang, S. H.; Slater, M.; Rood, S.; Vaughey, J. T.; Karan, N.; Balasubramanian, M.; Johnson, C. S. Enabling Sodium Batteries Using Lithium-Substituted Sodium Layered Transition Metal Oxide Cathodes. *Adv. Energy Mater.* **2011**, *1*, 333−336.

(14) Berthelot, R.; Carlier, D.; Delmas, C. Electrochemical Investigation of the P2−Na_xCoO_2 Phase Diagram. *Nat. Mater.* **2011**, *10*, 74−80.

(15) Caballero, A.; Hernan, L.; Morales, J.; Sanchez, L.; Santos, P. J.; Aranda, M. A. G. Synthesis and Characterization of high-temperature hexagonal P2-$Na_{0.6}MnO_2$ and Its Electrochemical Behaviour as a Cathode in Sodium Cells. *J. Mater. Chem.* **2002**, *12*, 1142−1147.

(16) Tripathi, R.; Wood, S. M.; Islam, M. S.; Nazar, L. F. Na-Ion Mobility in Layered Na_2FePO_4F and Olivine $Na[Fe,Mn]PO_4$. *Energy Environ. Sci.* **2013**, *6*, 2257.

(17) Jian, Z.; Han, W.; Lu, X.; Yang, H.; Hu, Y.-S.; Zhou, J.; Zhou, Z.; Li, J.; Chen, W.; Chen, D.; Chen, L. Superior Electrochemical Performance and Storage Mechanism of $Na_3V_2(PO_4)_3$ Cathode for Room-Temperature Sodium-Ion Batteries. *Adv. Energy Mater.* **2013**, *3*, 156−160.

(18) Barker, J.; Saidi, M. Y.; Sowyer, J. L. A Sodium-Ion Cell Based on the Fluorophosphate Compound $NaVPO_4F$. *Electrochem. Solid State Lett.* **2003**, *6*, A1−A4.

(19) Moreau, P.; Guyomard, D.; Gaubicher, J.; Boucher, F. Structure and Stability of Sodium Intercalated Phases in Olivine $FePO_4$. *Chem. Mater.* **2010**, *22*, 4126−4128.

(20) Lee, K. T.; Ramesh, T. N.; Nan, F.; Botton, G.; Nazar, L. F. Topochemical Synthesis of Sodium Metal Phosphate Olivines for Sodium-Ion Batteries. *Chem. Mater.* **2011**, *23*, 3593−3600.

(21) Oh, S. M.; Myungc, S. T.; Hassound, J.; Scrosati, B.; Sun, Y. K. Reversible $NaFePO_4$ Electrode for Sodium Secondary Batteries. *Electrochem. Commun.* **2012**, *22*, 149−152.

(22) Ellis, B. L.; Makahnouk, W. R. M.; Makimura, Y.; Toghill, K.; Nazar, L. F. A Multifunctional 3.5 V Iron-Based Phosphate Cathode for Rechargeable Batteries. *Nat. Mater.* **2007**, *6*, 749−753.

(23) Recham, N.; Chotard, J. N.; Dupont, L.; Djellab, K.; Armand, M.; Tarascon, J. M. Ionothermal Synthesis of Sodium-Based Fluorophosphate Cathode Materials. *J. Electrochem. Soc.* **2009**, *156*, A993−A999.

(24) Kawabe, Y.; Yabuuchi, N.; Kajiyama, M.; Fukuhara, N.; Inamasu, T.; Okuyama, R.; Nakai, I.; Komaba, S. Synthesis and Electrode Performance of Carbon Coated Na_2FePO_4F for Rechargeable Na Batteries. *Electrochemistry* **2011**, *13*, 1225−1228.

(25) Nose, M.; Nobuhara, K.; Nakayama, S. S. H.; Nakanshi, S.; Iba, H. Electrochemical Li^+ Insertion Capabilities of $Na_{4−x}Co_3(PO_4)_2P_2O_7$ and Its Application to Novel Hybrid-Ion Batteries. *RSC Adv.* **2014**, *4*, 9044.

(26) Kim, H.; Park, I.; Lee, S.; Kim, H.; Park, K.-Y.; Park, Y.-U.; Kim, H.; Kim, J.; Lim, H.-D.; Yoon, W.-S.; Kang, K. Understanding the Electrochemical Mechanism of the New Iron-Based Mixed-Phosphate $Na_4Fe_3(PO_4)_2P_2O_7$ in a Na Rechargeable Battery. *Chem. Mater.* **2013**, *25*, 3614−3622.

(27) Kim, H.; Park, I.; Seo, D. H.; Lee, S.; Kim, S. W.; Kwon, W. J.; Park, Y. U.; Jeon, C. S. K. S.; Kang, K. New Iron-Based Mixed-Polyanion Cathodes for Lithium and Sodium Rechargeable Batteries: Combined First Principles and Experimental Study. *J. Am. Chem. Soc.* **2012**, *134*, 10369−10372.

(28) Tripathi, R.; Ramesh, T. N.; Ellis, B. L.; Nazar, L. F. Scalable Synthesis of Tavorite $LiFeSO_4F$ and $NaFeSO_4F$ Cathode Materials. *Angew. Chem., Int. Ed.* **2010**, *49*, 8738−8742.

(29) Catlow, C. R. *Computer Modelling in Inorganic Crystallography*; Academic Press: San Diego, CA, 1997.

(30) Gale, J. D. GULP: A Computer Program for the Symmetry-Adapted Simulation of Solids. *J. Chem. Soc., Faraday Trans.* **1997**, *93*, 629−637.

(31) Catlow, R. *Computational Approaches to Energy Materials*; Wiley: Chichester, U.K., 2013.

(32) Islam, M. S.; Driscoll, D. J.; Fisher, C. A. J.; Slater, P. R. Atomic-Scale Investigation of Defects, Dopants, and Lithium Transport in the $LiFePO_4$ Olivine-Type Battery Material. *Chem. Mater.* **2005**, *17*, 5085−5092.

(33) Clark, J. M.; Nishimura, S.; Yamada, A.; Islam, M. S. High-Voltage Pyrophosphate Cathode: Insights into Local Structure and Lithium-Diffusion Pathways. *Angew. Chem., Int. Ed.* **2012**, *51*, 13149−13153.

(34) Armstrong, A. R.; Lyness, C.; Panchmatia, P. M.; Islam, M. S.; Bruce, P. G. The Lithium Intercalation Process in the Low-Voltage Lithium Battery Anode $Li_{1+x}V_{1−x}O_2$. *Nat. Mater.* **2011**, *10*, 223−229.

(35) Andreev, Y. G.; Panchmatia, P. M.; Parker, S. C.; Islam, M. S.; Bruce, P. *J. Am. Chem. Soc.* **2014**, *136*, 6306−6312.

(36) Clark, J. M.; Barpanda, P.; Yamada, A.; Islam, M. S. Sodium Ion Battery Cathodes $Na_2FeP_2O_7$ and $Na_2MnP_2O_7$: Diffusion Behaviour for High Rate Performance. *J. Mater. Chem. A* **2014**, *2*, 11807−11812.

(37) Todorov, I. T.; Smith, W.; Trachenko, K.; Dove, M. T. DL_POLY_3: New Dimensions in Molecular Dynamics Simulations via Massive Parallelism. *J. Mater. Chem.* **2006**, *16*, 1911−1918.

(38) Pedone, A.; Malavasi, G.; Menziani, M. C.; Cormack, A. N.; Segre, U. A New Self-Consistent Empirical Interatomic Potential Model for Oxides, Silicates and Silica-Based Glasses. *J. Phys. Chem. B* **2006**, *110*, 11780−11795.

(39) Lee, S.; Park, S. S. Atomistic Simulation Study of Mixed-Metal Oxide $Li(Ni_{1/3}Co_{1/3}Mn_{1/3})O_2$ Cathode Material for Lithium Ion Battery. *J. Phys. Chem. C* **2012**, *116*, 6484−6489.

(40) Tealdi, C.; Spreafico, C.; Mustarelli, P. Lithium Diffusion in $Li_{1−x}FePO_4$: The Effect of Cationic Disorder. *J. Mater. Chem.* **2012**, *22*, 24870−24876.

(41) Slanne, M.; Marrochelli, M.; Watson, G. W. Cooperative Mechanism for the Diffusion of Li^+ Ions in $LiMgSO_4F$. *J. Phys. Chem. C* **2012**, *116*, 18618−18625.

(42) Panchmatia, P. M.; Orera, A.; Rees, G. J.; Smith, M. E.; Hanna, J. V.; Slater, P. R.; Islam, M. S. Oxygen Defects and Novel Transport Mechanisms in Apatite Ion Conductors: Combined ^{17}O NMR and Modelling Studies. *Angew. Chem., Int. Ed.* **2011**, *123*, 9500−9505.

(43) Panchmatia, P. M.; Armstrong, A. R.; Bruce, P. G.; Islam, M. S. Lithium-Ion Diffusion Mechanisms in the Battery Anode Material $Li_{1+x}V_{1-x}O_2$. *Phys. Chem. Chem. Phys.* **2014**, *16*, 21114−21118.

(44) Kresse, G.; Furthermuller, J. Effective Iterative Schemes for Ab-Initio Total-Energy Calculations Using a Plane Wave Basis Set. *Phys. Rev. B: Condens. Matter Mater. Phys.* **1996**, *54*, 11169.

(45) Blochl, P. E. Projector Augmented Wave Method. *Phys. Rev. B: Condens. Matter Mater. Phys.* **1994**, *50*, 17953.

(46) Kresse, G.; Joubert, D. From Ultrasoft Pseudopotentials to the Projector Augmented Wave Method. *Phys. Rev. B: Condens. Matter Mater. Phys.* **1999**, *59*, 1758.

(47) Perdew, J. P.; Burke, K.; Ernzerhof, M. Generalized Gradient Approximation Made Simpe. *Phys. Rev. Lett.* **1996**, *77*, 3865.

(48) Jain, A.; Hautier, G.; Moore, C. J.; Ong, S. P.; Fischer, C. C.; Mueller, T.; Persson, K. A.; Ceder, G. A High Throughput Infrastructure for Density Functional Theory Calculations. *Comput. Mater. Sci.* **2011**, *50*, 2295−2310.

(49) Eames, C.; Clark, J. M.; Rousse, G.; Tarascon, J.-M.; Islam, M. S. Lithium Migration Pathways and van der Waal Effects in the $LiFeSO_4OH$ Battery Material. *Chem. Mater.* **2014**, *26*, 3672−3678.

(50) Clark, J. M.; Eames, C.; Reynaud, M.; Rousse, G.; Chotard, J. N.; Tarascon, J. M.; Islam, M. S. High Voltage Sulphate Cathodes $Li_2M(SO_4)_2$ (M = Fe, Mn, Co): Atomic-Scale Studies of Lithium Diffusion, Surfaces and Voltage Trends. *J. Mater. Chem. A* **2014**, *2*, 7446−7453.

(51) Arrouvel, C.; Parker, S. C.; Islam, M. S. Lithium Insertion and Transport in the TiO_2-B Anode Material: A Computational Study. *Chem. Mater.* **2009**, *21*, 4778−4783.

(52) Sanz, F.; Parada, C.; Rojo, J. M.; Valero, C. R. Synthesis, Structural Characterization, Magnetic Properties, and Ionic Con-

ductivity of $Na_4M^{II}_3(PO_4)_2P_2O_7$ (M^{II} = Mn, Co, Ni). *Chem. Mater.* **2001**, *13*, 1334−1340.

(53) Frederikse, H. P. R. *CRC Handbook of Chemistry and Physics*; CRC Press: Boca Raton, FL, 2005.

(54) Armstrong, A. R.; Kuganathan, N.; Islam, M. S.; Bruce, P. G. Structure and Lithium Transport Pathways in Li_2FeSiO_4 Cathodes for Lithium Batteries. *J. Am. Chem. Soc.* **2011**, *133*, 13031−13035.

(55) Shibata, T.; Kobayash, W.; Moritomo, Y. Sodium Ion Diffusion in Layered Na_xMnO_2 (0.49 < x < 0.75): Comparison with Na_xCoO_2. *Appl. Phys. Express* **2014**, *7*, 067101.

(56) Jiang, T.; Chen, G.; Li, A.; Wang, C.; Wei, Y. Sol−Gel Preparation and Electrochemical Properties of $Na_3V_2(PO_4)_2F_3$/C Composite Cathode Material for Lithium Ion Batteries. *J. Alloys Compd.* **2009**, *478*, 604−607.

(57) Ong, S. P.; Chevrier, V. L.; Hautier, G.; Jain, A.; Moore, C.; Kim, S.; Ma, X.; Ceder, G. Voltage, Stability and Diffusion Barrier Differences between Sodium-Ion and Lithium-Ion Intercalation Materials. *Energy Environ. Sci.* **2011**, *4*, 3680−3688.

(58) Yamada, A.; Hosoya, M.; Chung, S.-C.; Kudo, Y.; Hinokuma, K.; Liu, K.-Y.; Nishi, Y. Olivine-Type Cathodes: Achievements and Problems. *J. Power Sources* **2003**, *119*, 232−238.

(59) Wolfenstine, J.; Allen, J. Ni^{3+}/Ni^{2+} Redox Potential in $LiNiPO_4$. *J. Power Sources* **2005**, *142*, 389−390.

(60) Tamaru, M.; Barpanda, P.; Yamada, Y.; Nishimura, S.; Yamada, A. Observation of the Highest Mn^{3+}/Mn^{2+} Redox Potential of 4.45 V in a $Li_2MnP_2O_7$ Pyrophosphate Cathode. *J. Mater. Chem.* **2012**, *22*, 24526−24529.

(61) Wu, X.; Zheng, J.; Gong, Z.; Yang, Y. Sol−Gel Synthesis and Electrochemical Properties of Fluorophosphates $Na_2Fe_{1−x}Mn_xPO_4F$/C (x = 0, 0.1, 0.3, 0.7, 1) Composite as Cathode Materials for Lithium Ion Battery. *J. Mater. Chem.* **2011**, *21*, 18630−18637.